Journal of Colloid and Interface Science 604 (2021) 350–357

Contents lists available at ScienceDirect

Journal of Colloid and Interface Science

journal homepage: www.elsevier.com/locate/jcis

The role of mixed alkali metal cations on the formation of nanosized CHA zeolite from colloidal precursor suspension

Sajjad Ghojavand [a], Edwin B. Clatworthy [a], Aurélie Vicente [a], Eddy Dib [a], Valérie Ruaux [a], Maxime Debost [a,b], Jaafar El Fallah [a], Svetlana Mintova [a,*]

[a] Normandie Université, ENSICAEN, UNICAEN, CNRS, Laboratoire Catalyse et Spectrochimie (LCS), 14000 Caen, France
[b] Normandie Université, ENSICAEN, UNICAEN, CNRS, CRISMAT, 14000 Caen, France

GRAPHICAL ABSTRACT

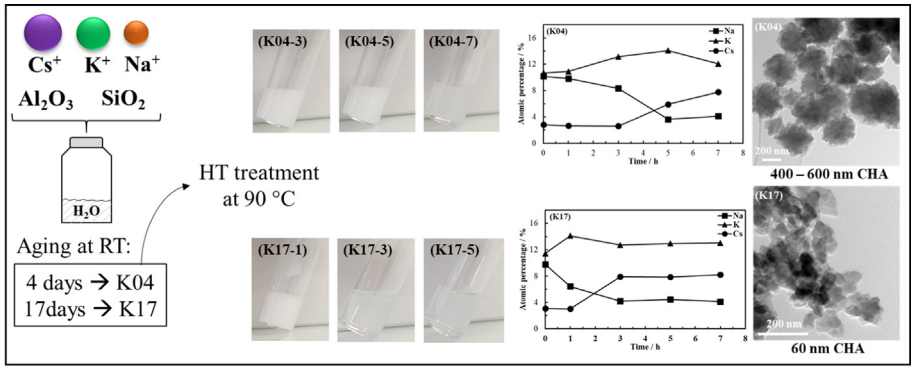

ARTICLE INFO

Article history:
Received 30 April 2021
Revised 8 June 2021
Accepted 30 June 2021
Available online 6 July 2021

Keywords:
Nanozeolite
Chabazite
Colloidal suspension
Crystallization
Organic template-free
Inorganic cation templating

ABSTRACT

A clear understanding of the crystal formation pathways of zeolites remains one of the most challenging issues to date. Here we investigate the synthesis of nanosized chabazite (CHA) zeolites using organic template-free colloidal suspensions by varying the time of aging at room temperature and the time of hydrothermal treatment at 90 °C. The role of mixed alkali metal cations (Na^+, K^+, Cs^+) on the formation of CHA in the colloidal suspensions was studied. Increasing the aging time of the precursor colloidal suspension from 4 to 17 days resulted in faster crystallization of CHA nanocrystals (3 h instead of 7 h at 90 °C) to afford significantly smaller particles (60 nm *vs* 600 nm). During the crystallization a considerable change in the content of inorganic cations in the recovered solid material was observed to coincide with the formation of the CHA nanocrystals. The Na^+ cations were found to direct the formation of condensed and pre-shaped aluminosilicate particles in the colloidal precursor suspensions, while K^+ cations facilitated the formation of secondary building units (SBUs) of the CHA type framework structure such as *d6r* and *cha* cages, and the Cs^+ cations promoted the long-range crystalline order facilitating the crystallization of stable zeolite nanocrystals.

* Corresponding author.
E-mail address: svetlana.mintova@ensicaen.fr (S. Mintova).

https://doi.org/10.1016/j.jcis.2021.06.176
0021-9797/

1. Introduction

Zeolites play a critical role in industrial applications such as separation and catalysis due to their molecular-sized pore openings (0.3–2 nm) and shape selectivity [1–4]. Zeolites consist of ordered corner-sharing TO_4 tetrahedra (typically T = Si, Al) which can be arranged to produce a variety of different frameworks allowing for the tuning of their chemical and physical properties [5,6]. The particle size of conventional zeolites are typically in the order of micrometers and are composed of aggregates of several individual crystals [7]. Due to their size one of the major drawbacks of conventional zeolites is diffusion limitations, however, this can be addressed by decreasing the zeolite particle size [8]. Nanosized zeolites have dimensions of less than 200 nm and unlike conventional zeolites are typically composed of discrete particles (single crystals), exhibit greater external surface area, and possess a greater number of available active sites [5,7,9].

There are several methods for synthesizing nanozeolites including from clear suspensions [10,11], using crystal growth inhibitors [12], confined space synthesis [13,14], and from organic solvents [15,16]. Features shared across these synthesis methods include the use of a basic synthesis media, an organic structure-directing agent (OSDA), and amorphous sources of silica and alumina. The formation of nanozeolites is typically achieved by heating the reaction mixture in a sealed reactor [9]. However, nanozeolites synthesized using OSDAs have a relatively high cost, toxicity due to the presence of organic templates, and require a post-synthetic calcination that can cause partial collapse of the zeolite structure and necessitates additional energy and release of CO_2 [5]. A promising alternative for the synthesis of nanozeolites is the organic template-free method [17]. In this method the ionic interactions of cations with SiO_4^{4-} and AlO_4^{5-} tetrahedra are used to direct the formation of the nanozeolites [5]. In addition, the nanozeolites are prepared at relatively low temperatures (*e.g.* <100 °C) to favor the uniform nucleation of particles with a similar size [5]. By careful tuning of the type and content of cations, aging time, and hydrothermal temperature, various zeolites with nanoscale dimensions have been synthesized without the use of OSDAs [3,17–19]. However, key aspects of the organic template-free method such as the crystal formation and the role of different cations in directing the zeolite structure require further investigation.

We recently reported the synthesis of nanosized chabazite (CHA) using a highly alkaline mixture containing three monovalent alkali metal cations as templates (Na^+, K^+, and Cs^+) [20]. The CHA framework is described by a three-dimensional pore system containing super cages of 6.7 × 10 Å which are accessed by eight-membered rings (8MRs) of 3.8 × 3.8 Å [21]. Here, we describe the crystal formation in two series of samples from colloidal precursor suspensions by varying the aging time and the synthesis time resulting in nanosized CHA zeolites with different particle sizes (60 nm and 600 nm). The role of the mixed inorganic cations in directing the CHA structure was identified using a combination of ICP-MS and EDX analyses.

2. Experimental

2.1. Materials and synthesis

All reagents were used as received unless otherwise specified. Sodium hydroxide pellets (98 wt%), potassium hydroxide (85 wt %), LUDOX AS-40, and sodium aluminate ($NaAlO_2$, 40–45% Na_2O, 50–56% Al_2O_3) were purchased from Sigma-Aldrich. Cesium hydroxide hydrate (15–20 wt% H_2O) was purchased from Alfa Aesar. Double distilled (dd) water was used for all syntheses. Synthesis of the CHA samples was based on a modified protocol published recently by our group [20]. 0.54 g of $NaAlO_2$ was mixed with 4.4 g of water under rapid stirring. After obtaining a clear suspension, 1.7 g of NaOH, 0.824 g of KOH, and 0.217 g of CsOH (50 wt% Cs in water) were added and stirred for 2 h to obtain a clear solution. Afterwards, 10 g of LUDOX AS-40 was added dropwise under rapid stirring. The final colloidal suspension precursor composition was $0.2Cs_2O$: $1.5K_2O$: $6.0Na_2O$: $16.0SiO_2$: $0.7Al_2O_3$: $141.7H_2O$ Two series of samples were prepared whereby the colloidal precursor suspensions were aged at room temperature with vigorous stirring for either 4 days (K04 series) or 17 days (K17 series). Hydrothermal (HT) treatment of the colloidal precursor suspensions was performed in a static oven at 90 °C for up to 9 h. After HT treatment the solid material was recovered by centrifugation and washed with hot water (90 °C) until neutral pH (7–8) of the decanted solution was achieved. The recovered material was dried in an oven at 60 °C overnight. The samples obtained from the series K04 after 1, 3, 5, 7, and 9 h of HT treatment are abbreviated as K04-1, -3, -5, -7, and -9, while the samples from series K17 after 1, 3, 5, and 7 h of HT treatment are abbreviated as K17-1, -3, -5, and -7.

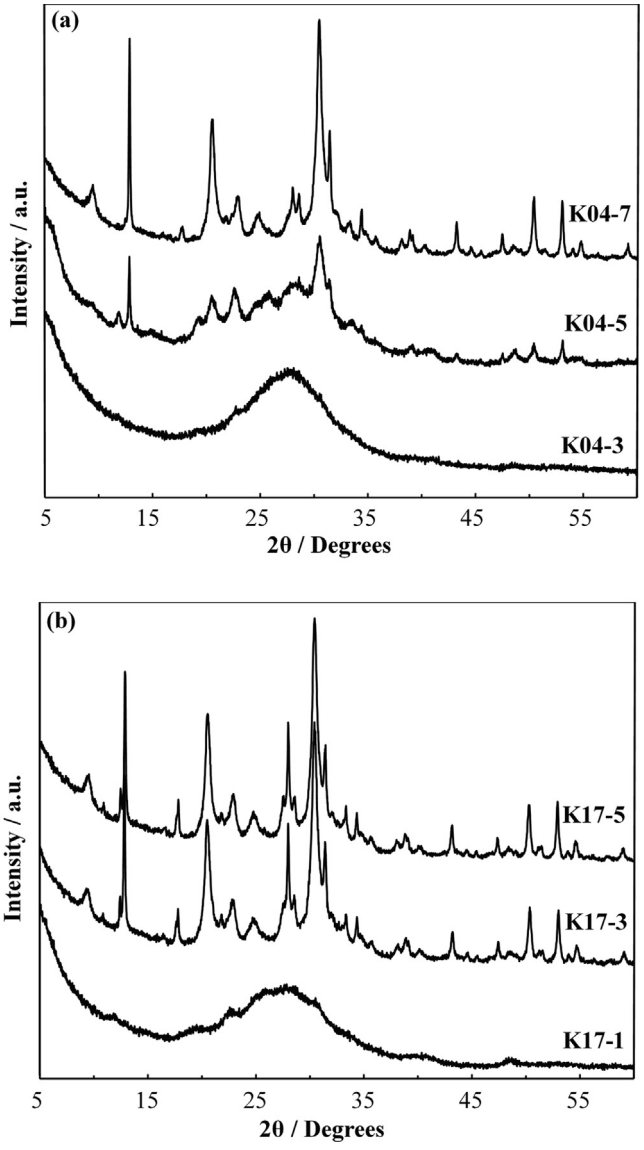

Fig. 1. XRD patterns of the nanosized CHA samples (a) K04-3, K04-5, and K04-7 (b) K17-1, K17-03, and K17-5 synthesized from colloidal precursor suspensions aged four and seventeen days, respectively.

2.2. Sample characterization

Powder X-ray diffraction (XRD) patterns of zeolites were collected with a PANalytical X'Pert Pro diffractometer equipped with a Johansson monochromator using the Cu Kα1 radiation (λ = 1.54 0598 Å). Scanning electron microscopy (SEM) of samples was performed using a Tescan Mira I LMH under 20 kV. Energy dispersive X-ray (EDX) analysis of samples was performed using two Bruker XFLASH 6/30 EDX cameras. The crystal size and morphology of solids were determined by high-resolution transmission electron microscopy (HR-TEM) using a FEI LaB_6 TECNAI G2 30UT operated at 300 kV. Viscosity measurements of the colloidal suspension of series K04 and K17 were performed using a rotational rheometer from Kenexus and a PU20 SC0085 SS geometry.

Magic-angle spinning nuclear magnetic resonance (MAS NMR) spectra of ^{27}Al, ^{29}Si, and ^{133}Cs nuclei were recorded with a single pulse on a Bruker Avance 400 MHz (9.4 T) spectrometer using 4 mm-OD zirconia rotors with a spinning frequency of between 12 and 14 kHz. Details are listed in Table S2.

The FTIR spectra of samples were recorded with a Nexus IR spectrometer (1300–450 cm^{-1}, resolution of 1 cm^{-1}, 132 scans) using the KBr pellet technique. Inductively coupled plasma mass spectrometry (ICP-MS) measurements were recorded using a 7900 ICP-MS from Agilent Technologies.

3. Results and discussion

3.1. Macroscopic characterization of nanosized CHA zeolites

The XRD patterns of the samples from the K04 and K17 series are presented in Fig. 1. For the K04-5 sample, the XRD pattern reveals the emergence of the diffraction peaks associated with the CHA framework structure indicating that the formation of the CHA structure begins after approximately 3 h of HT treatment of the colloidal precursor suspension at 90 °C. Even after 5 h of HT treatment the diffraction peaks are broad and display low intensity signifying that a large amount of amorphous precursor material is still present. Increasing the time of HT treatment showed that fully crystalline CHA was obtained after 7 h; no further changes were observed in the XRD patterns at longer HT treatment times (Fig. S1). In comparison, for the K17 series the CHA structure is formed after 3 h of HT treatment showing that increasing of the aging time of the colloidal suspension leads to faster crystallization of the CHA zeolite. The fully crystalline CHA zeolite is formed more rapidly in the K17 series as evidenced by the identical XRD patterns for samples K17- 3, -5 and -7 (Fig. S2).

Microscopic analysis of CHA samples from the K04 and K17 series revealed clear morphological differences between them as a result of the different aging times. Fig. 2 presents SEM images of the K04 and K17 samples showing the transformation from amorphous matter to crystalline CHA zeolite over the 7 h of HT treatment. Sample K04-3 (Fig. 2a) consists of micron-sized amorphous agglomerated aluminosilicate particles while after 5 h of HT treatment crystalline CHA particles can be seen together with amorphous material (Fig. 2b). The CHA particles have an average size of ≈600 nm in diameter while the amorphous material exhibits micrometer sized particles. After 7 h of HT treatment all of the amorphous material converts to crystalline CHA particles ≈600 nm in diameter with morphology defined by rough spheres of smaller intergrown crystallites (Fig. 2c). For the K17 series, sample K17-1 shows similar amorphous appearance to sample K04-3 (Fig. 2d). However, sample K17-3 consists of fully crystalline nanosized CHA crystals 60 nm across (Fig. 2e). This is consistent with the appearance of the Bragg peaks of the CHA structure after 3 h of HT treatment of the colloidal precursor suspension presented in Fig. 1b. Increasing the HT treatment beyond 3 h does not affect the size or morphology of the CHA nanocrystals (K17-5, Fig. 2f), which is consistent with the XRD results (Fig. 1).

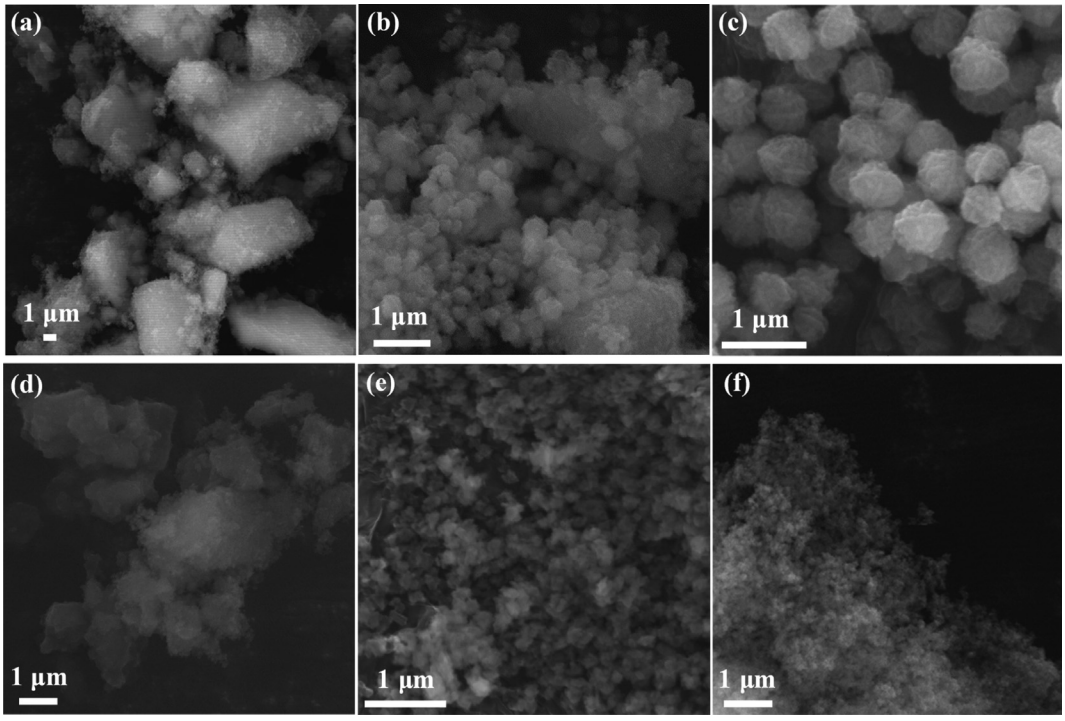

Fig. 2. SEM images of the nanosized CHA samples (a) K04-3, (b) K04-5, and (c) K04-7 and samples (d) K17-1, (e) K17-3, and (f) K17-5 synthesized from colloidal precursor suspensions aged four and seventeen days, respectively.

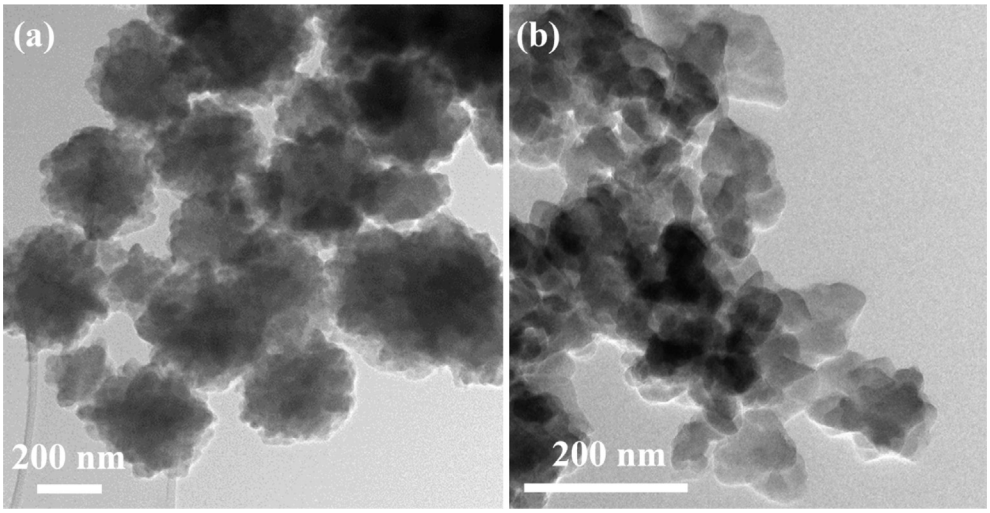

Fig. 3. TEM images highlighting the morphology of fully crystalline nanosized CHA samples (a) K04-7 and (b) K17-3.

TEM analysis was also performed on the fully crystalline samples K04-7 and K17-3 (Fig. 3). The TEM image for the sample K04-7 clearly shows that the particles are primarily between 400 and 600 nm in size and are composed of smaller polycrystalline intergrown crystallites (Fig. 3a), consistent with the SEM results. Smaller particles (<200 nm) with similar morphology were also observed. In comparison, TEM analysis of the sample K17-3 shows discrete nanosized CHA crystals with sizes of less than 60 nm (Fig. 3b) significantly smaller than the CHA reported in our previous work (~200 nm) [20].

Rheometric analysis of the CHA samples from the K04 and K17 series are presented in Fig. 4 showing the changes in the viscosity of the colloidal precursor suspension during the HT treatment. As shown in Fig. 4a for sample K04-1, the viscosity of the colloidal suspension increases substantially from 2 cPs to 50,000 cPs and remains high until 3 h of HT treatment due to the formation of micron-sized amorphous agglomerated aluminosilicate particles (Fig. 2a). Only after 5 h of HT treatment does the viscosity value decrease (from 46,000 cPs to 7500 cPs) due to the transformation of the large amorphous agglomerates to smaller CHA crystals (Fig. 1a and Fig. 2b). Increasing the HT treatment to 7 h transforms all of the micron-sized amorphous agglomerates into crystalline CHA particles (shown in Fig. 2c) and the viscosity decreases significantly from 7500 cPs to 0.9 Cps. In comparison, the viscosity of the K17 series changes over a shorter period of time. Sample K17-1 shows a high viscosity similar to K04-3 followed by a significant reduction in viscosity after 3 h of HT treatment due to the transformation of the colloidal precursor suspension into crystalline nanosized CHA (Fig. 1b, Fig. 2e, and Fig. 3b). The significant changes (increase followed by decrease) in viscosity of the colloidal suspension during the crystallization process can be attributed to the polymerization of the cation-coordinated SiO_4^{4-} and AlO_4^{5-} tetrahedra followed by the establishment of long-range crystallinity facilitated by the dynamic changes in the cation content between the solid and liquid phases in the colloidal suspension (*vide infra*).

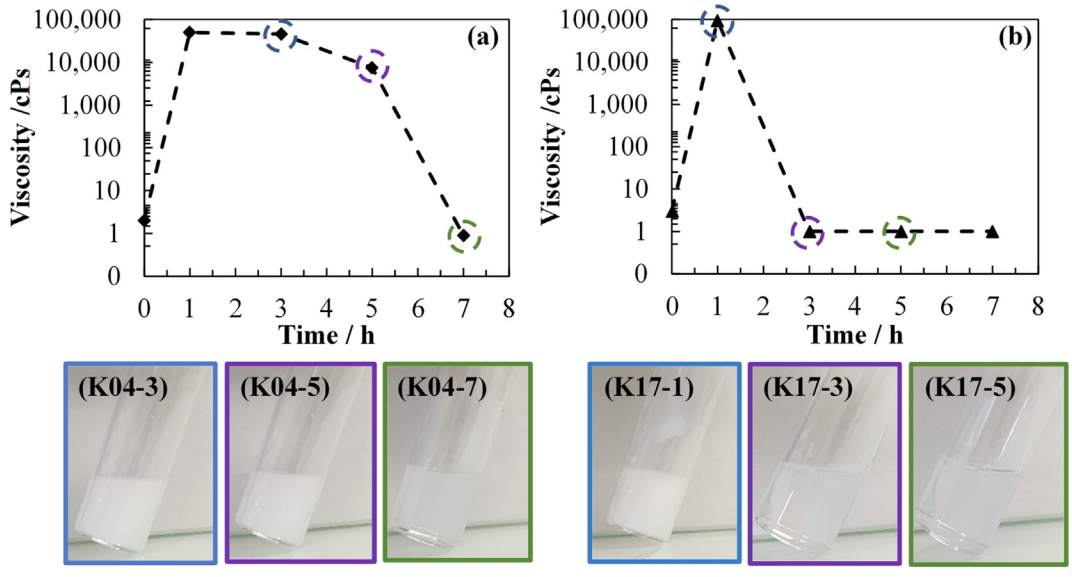

Fig. 4. Top: viscosity changes of the colloidal precursor suspensions of samples from the series K04 and K17 at different times of hydrothermal treatment: (a) K04-0, K04-1, K04-3, K04-5, and K04-7, and (b) K17-0, K17-1, K17-3, K17-5, and K17-7. Bottom: pictures of the colloidal suspensions K04-3, K04-5, K04-7, K17-1, K17-3, and K17-5.

3.2. Spectroscopic characterization of nanosized CHA zeolites

To further understand the evolution of the colloidal precursor suspensions and the formation of the CHA zeolite during the crystallization process, the two series of samples were analyzed by FTIR and NMR spectroscopy. The FTIR spectra of the K04 and K17 series of samples in the range of 450–1300 cm^{-1} are presented in Fig. 5. The formation of the secondary building units (SBUs) relative to the CHA zeolite during the crystallization process was studied. A broad vibration band related to the asymmetric stretching of Si–O–T (T = Al or Si) can be seen at 950–1200 cm^{-1} for all samples [22,23], while the symmetric vibration of Si–O–T also appears at 670–820 cm^{-1} [24,25]. This suggests that prior to the detection of the long-range crystalline order in the CHA zeolite observable by XRD, polymerization of silica and alumina resulting in the formation of amorphous aluminosilicates possessing short range crystalline order (*i.e.* crystal nuclei) is observed by FTIR spectroscopy. In the K04 series, the sample K04-5 contains a peak at 466 cm^{-1} corresponding to the O–Si–O bending mode [26,27]. After 7 h two new bands at 518 and 635 cm^{-1} appeared which can be attributed to double six-membered rings (*d6r*) and the 8MR as a secondary building unit (SBU) in the *cha* cage, respectively. In comparison, in the spectrum of sample K17-3 the shoulder at 466 cm^{-1} attributed to the O–Si–O bending mode is already present. Both the *d6r* and 8MR bands also appear in the spectrum of sample K17-3 and remain relatively unchanged with further HT treatment of the colloidal suspensions (Fig. S3). These results suggest that the crystallization of the CHA zeolite starts with the formation of *d6r* and *cha* structures and that their further development into a long-range crystalline structure requires a template such as an appropriate organic or inorganic cation, or a mixture of both.

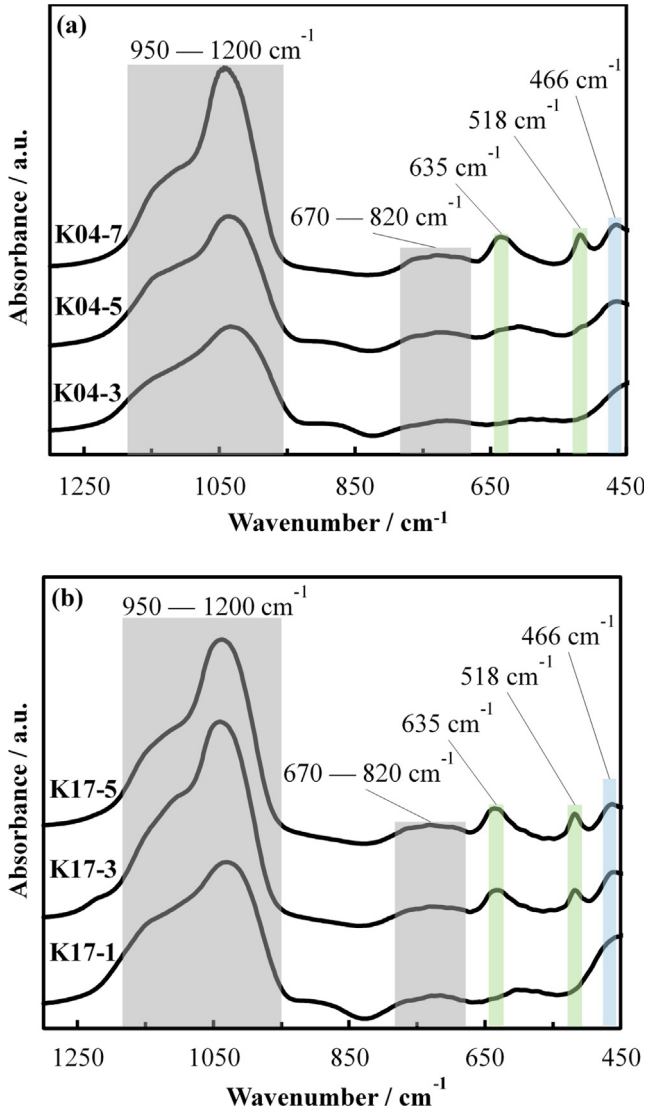

Fig. 5. FTIR spectra of the nanosized CHA samples: (a) K04-3, K04-5, and K04-7 and (b) K17-1, K17-3, and K17-5 synthesized from colloidal precursor suspensions aged four and seventeen days, respectively.

^{27}Al MAS NMR analysis of the K04 and K17 series were performed and the spectra are presented in Fig. 6a,b. All samples in these series show a resonance at 57 ppm which is related to the tetrahedrally coordinated Al atoms, and no signal corresponding to extra-framework Al is observed. This agrees with the appearance of Si–O–T (T = Al or Si) stretching and vibrational bands in the FTIR spectra presented in Fig. 5, suggesting the formation of a polymerized aluminosilicate amorphous or crystalline (depending on the HT treatment time) species after aging of the samples. For the K04 series (Fig. 6a), sample K04-3 shows a broad asymmetric resonance which suggests a heterogeneous surrounding of Al typical of amorphous aluminosilicates which is consistent with XRD pattern presented in Fig. 1a. Increasing the HT treatment to 5 h sharpens the resonance while 7 h of HT treatment reveals a more intense sharp symmetric resonance related to the fully crystalline tetrahedral Al. For the K17 series (Fig. 6b) the sample K17-1 shows an asymmetric resonance in the ^{27}Al spectrum related to the amorphous aluminosilicates observed similarly in sample K04-3. However, after 3 h of HT treatment the ^{27}Al spectrum reveals a symmetric resonance at 57 ppm typical of crystalline structures. The band at 57 ppm does not change with increasing the HT treatment time to 5 h. These results are consistent with the XRD, electron microscopy and FTIR analyses.

^{29}Si MAS NMR analysis for the K04 and K17 series are presented in Fig. 6c,d. Samples K04-3 and K04-5 show asymmetric broad resonances from −110 ppm to −80 ppm which suggests a complex heterogeneous tetrahedrally coordinated Si atom in amorphous aluminosilicates (Fig. 6c). In comparison, sample K04-7 displays four resonances at −94, −99, −104, and −110 ppm correspond to 3 Al ($Si[SiO][AlO]_3$), 2 Al ($Si[SiO]_2[AlO]_2$), 1 Al ($Si[SiO]_3[AlO]$), and 0 Al ($Si[SiO]_4$) species [20]. For the K17 series (Fig. 6d), sample K17-1 shows similar results to the samples K04-3 and K04-5 while for samples K17-3 and K17-5 the different crystallographic Si environments can be observed and are similar to those of sample K04-7. The increased HT treatment from 3 h to 5 h does not result in any changes in the ^{29}Si NMR spectra for the K17 series, similar to the results shown for XRD and FTIR, thus confirming that fully crystalline CHA was obtained after 3 h. The Si/Al ratio of the fully crystalline samples K04-7 and K17-3 calculated by the Engelhardt and Michel equation is 2.1 (Table 1, S1). For comparison the Si/Al ratio of the samples obtained from ICP-MS and EDX are presented [28]. As shown, the Si/Al ratio of the fully crystalline samples (K04-7 and K17-3) is similar, which suggests a similar amount of alkali metal cations are present.

To study the placement and migration of the extra-framework cations ^{133}Cs MAS NMR analyses were performed on amorphous, semicrystalline, and crystalline samples from both series of CHA zeolites synthesized from the colloidal suspensions (Fig. S4). ^{133}Cs MAS NMR spectra reveal a symmetric resonance at −61 ppm in samples K04-5, K04-7, K17-3, and K17-5. This is assigned to a single Cs^+ extra-framework site located in the middle of the 8MR opening of the CHA structure, consistent with our previous results [20]. A separate study dedicated to understanding the exact location and dynamics of the Na^+ cations using ^{23}Na MQMAS NMR and Rietveld analyses will be presented in future work.

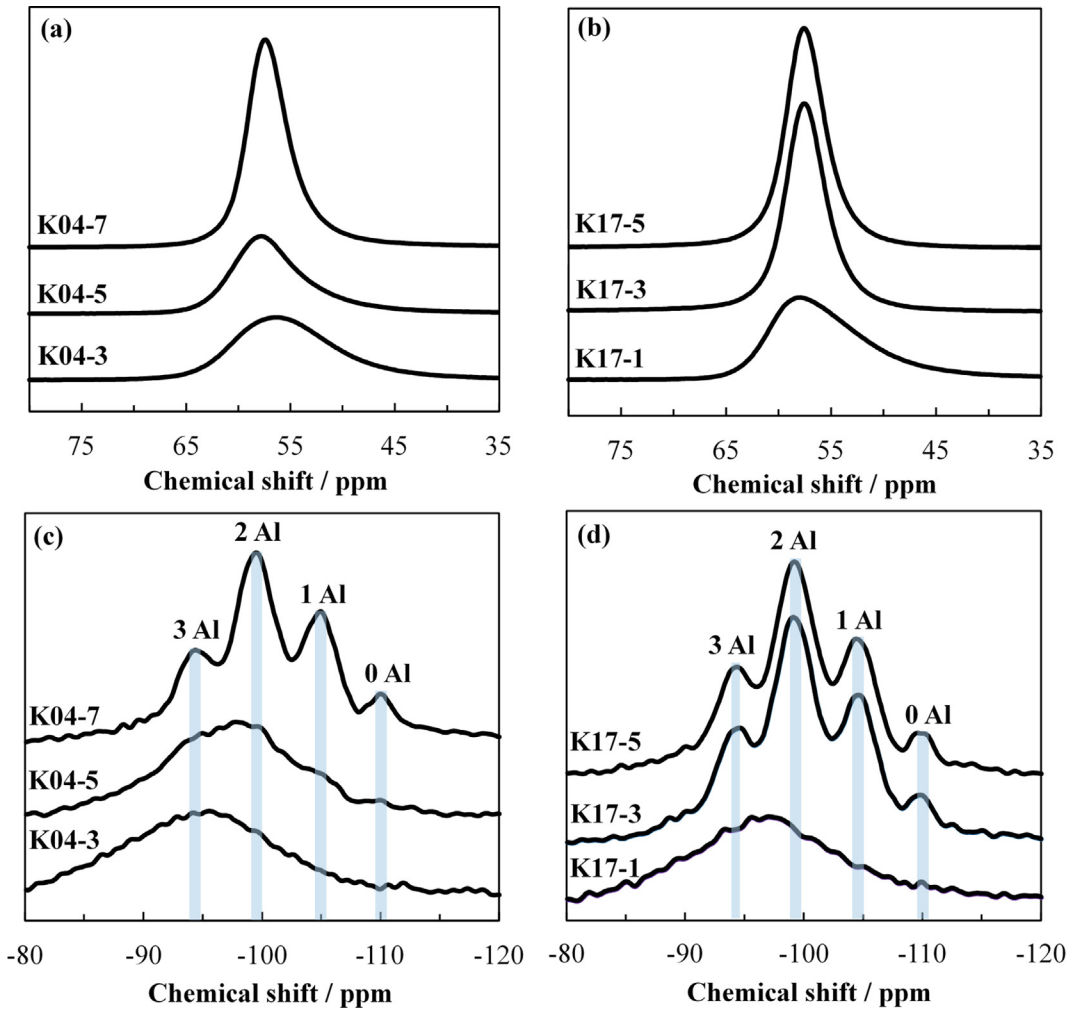

Fig. 6. ^{27}Al MAS NMR spectra of the nanosized CHA samples (a) K04-3, K04-5, and K04-7, (b) K17-1, K17-3, and K17-5. ^{29}Si MAS NMR spectra of CHA samples (c) K04-3, K04-5, and K04-7, (d) K17-1, K17-3, and K17-5 of CHA samples.

Table 1
Si/Al ratio of fully crystalline CHA samples (K04-7 and K17-3) based on ^{29}Si MAS NMR, ICP-MS, and EDX.

Set	Si/Al (^{29}Si NMR)	Si/Al (ICP-MS)	Si/Al (EDX)
K04-7	2.1	2.0	2.5
K17-3	2.1	1.9	2.5

In addition to determining the Si/Al ratio, the content of the extra-framework cations used to template the CHA structure was measured by ICP-MS and EDX. The atomic percentage of extra-framework cations (Na^+, K^+, Cs^+) in the recovered solid material of the K04 and K17 series based on ICP-MS is presented in Fig. 7. For the K04 series (Fig. 7a), the Na^+ content decreases consistently until 5 h, coincident with an increase in the K^+ cation content to its maximum value. The Cs^+ content begins increasing after approximately 3 h of HT treatment at which time the crystallization of the CHA structure begins. Beyond 5 h the K^+ content decreases slightly, coincident with a continued increase in the Cs^+ content and further crystallization of the CHA until 7 h. These results suggest that the high Na^+ content is required to stabilize the colloidal precursor suspension containing amorphous nanosized particles. The K^+ cations direct the formation of SBUs such as the *d6r*s and 8MRs of the CHA type framework. After the formation of the SBUs in sample K04-5, the first CHA crystals are observed (see Fig. 2b, Fig. 5a). During the crystallization, the Cs^+ partially replaces the Na^+ and K^+ cations leading to the formation of long-range crystalline matter, where a sufficient connectivity between the SBUs is achieved leading to the formation of fully crystalline CHA zeolite crystals (sample K04-7), see Fig. 1a and Fig. 7a. The same trend in the K17 series is observed. The changes in the cation content in the K17 series are corroborated with the macroscopic and spectroscopic results (Fig. 1b and Fig. 5b). The ICP-MS results are in good agreement with the EDX data (Supplementary Information, Fig. S5).

The role of the mixed inorganic cations used for the synthesis of CHA zeolite is presented schematically in Scheme S1. Initially, a colloidal precursor suspension containing a high concentration of inorganic cations (Na^+, K^+ and Cs^+) was stabilized at room temperature and subjected to aging at RT for 4 days (K04) and 17 days (K017). After 4 days of aging (K04 series), the colloidal precursor mixture contains large micron-sized amorphous aluminosilicates with a broad size distribution (Fig. 2a). After subjecting this colloidal precursor mixture to 5 h of HT treatment the content of K^+ and Cs^+ in the samples increases while the Na^+ decreases (Fig. 7a). K^+ cations promote the formation of different structures (*d6r* and 8MR), and due to the presence of Cs^+ cations the crystallization of the CHA type zeolite is accomplished. Increasing the HT

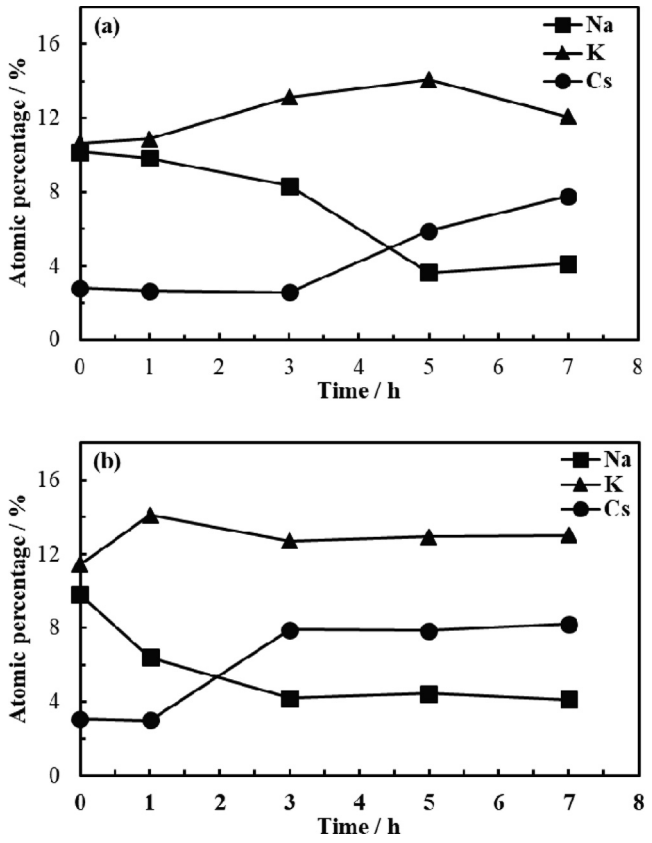

Fig. 7. ICP-MS analysis revealing the change in the content of extra-framework cations (Na^+, K^+, Cs^+) in the nanosized CHA series K04 and K17 at different times of hydrothermal treatment: (a) K04-0, K04-1, K04-3, K04-5, and K04-7, and (b) K17-0, K17-1, K17-3, K17-5, and K17-7.

treatment to 7 h (K04-7) induces further crystal growth resulting in CHA zeolite with a particle size of 600 nm. The CHA polycrystalline particles are composed of intergrown nanosized CHA crystals (Fig. 3a). In comparison, after 17 days of aging (K17 series) the colloidal precursor suspension contains smaller amorphous aluminosilicate particles in comparison to the K04 series (Fig. 2a, d). After 3 h of HT treatment the amorphous aluminosilicate particles transform into discrete nanosized CHA crystals with a size of less than 60 nm (Fig. 3b). The change in content of alkali metal cations in the recovered solid material is similar to the K04 series; a complete transformation from amorphous into crystalline particles is achieved within 3 h instead of 7 h compared to the K04 series (Fig. 1b and Fig. 7b). These results clearly highlight the important role of the inorganic cations in the synthesis of CHA zeolite nanocrystals.

4. Conclusions

The crystallization of nanosized CHA zeolite from colloidal precursor suspensions containing a high concentration of mixed inorganic structure-directing cations (Na^+, K^+ and Cs^+) subjected to room temperature aging for 4 and 17 days is reported. The crystallization kinetics, size, and morphology of the CHA crystals strongly depends on the aging time of the colloidal precursor suspensions. Four days of aging of the colloidal precursor suspension (K04 series) results in the formation of CHA zeolite composed of intergrown nanocrystals with a final particle size of 600 nm (7 h HT treatment at 90 °C). In comparison, it is assumed that the aging of the same colloidal precursor suspension for seventeen days (K17 series) resulted in the formation of monodispersed amorphous nanoparticles that transformed into CHA nanocrystals with a size of 60 nm (3 h HT treatment at 90 °C). The high concentration of mixed inorganic cations (Na^+, K^+, and Cs^+) is required to (i) solubilize the Si and facilitate stable colloidal suspensions containing amorphous particles enriched in Na^+, (ii) direct the formation of SBUs (*d6r*, 8MR) of the CHA type framework structure during the hydrothermal treatment by the high amount of K^+, and (iii) promote the formation of long-range crystalline order resulting in the crystallization of chabazite zeolite containing Cs^+ extra-framework cations. In combination with the factors of aging and HT treatment, understanding the role of inorganic cations in directing the formation of structural units and the crystallization of framework structures is critical to the development of intelligently designed porous materials with exceptional performance.

CRediT authorship contribution statement

Sajjad Ghojavand: Formal analysis, Investigation, Validation, Data curation, Writing - original draft, Visualization. **Edwin B. Clatworthy:** Validation, Data curation, Writing - review & editing. **Aurélie Vicente:** Investigation, Formal analysis. **Eddy Dib:** Investigation. **Valérie Ruaux:** Investigation. **Maxime Debost:** Formal analysis, Validation, Investigation. **Jaafar El Fallah:** Investigation. **Svetlana Mintova:** Supervision, Funding acquisition, Conceptualization, Data curation, Writing - review & editing.

Declaration of Competing Interest

The authors declare that they have no known competing financial interests or personal relationships that could have appeared to influence the work reported in this paper.

Acknowledgement

Financial support from the Normandy Region through the RIN Recherche Program (grant 18P01675) and the Industrial Chair ANR-TOTAL "Nanoclean Energy" (Grant IPA 5621) is acknowledged. Assistance of Dr. Cassandre Kouvatas and Dr. Hussein El Siblani in obtaining NMR data is also appreciated.

Appendix A. Supplementary material

Supplementary data to this article can be found online at https://doi.org/10.1016/j.jcis.2021.06.176.

References

[1] J. Shang, G. Li, R. Singh, Q. Gu, K.M. Nairn, T.J. Bastow, N. Medhekar, C.M. Doherty, A.J. Hill, J.Z. Liu, P.A. Webley, Discriminative Separation of Gases by a "Molecular Trapdoor" Mechanism in Chabazite Zeolites, J. Am. Chem. Soc. 134 (2012) 19246–19253, https://doi.org/10.1021/ja309274y.
[2] S.V. Konnov, F. Dubray, E.B. Clatworthy, C. Kouvatas, J.-P. Gilson, J.-P. Dath, D. Minoux, C. Aquino, V. Valtchev, S. Moldovan, S. Koneti, N. Nesterenko, S. Mintova, Novel Strategy for the Synthesis of Ultra-Stable Single-Site Mo-ZSM-5 Zeolite Nanocrystals, Angew. Chem. Int. Ed. 59 (2020) 19553–19560, https://doi.org/10.1002/anie.202006524.
[3] J. Grand, N. Barrier, M. Debost, E.B. Clatworthy, F. Laine, P. Boullay, N. Nesterenko, J.-P. Dath, J.-P. Gilson, S. Mintova, Flexible Template-Free RHO Nanosized Zeolite for Selective CO_2 Adsorption, Chem. Mater. 32 (2020) 5985–5993, https://doi.org/10.1021/acs.chemmater.0c01016.
[4] E.B. Clatworthy, S.V. Konnov, F. Dubray, N. Nesterenko, J.-P. Gilson, S. Mintova, Emphasis on the properties of metal-containing zeolites operating outside the comfort zone of current heterogeneous catalytic reactions, Angew. Chem. Int. Ed. 59 (2020) 19582–19600, https://doi.org/10.1002/anie.202005498.
[5] S. Mintova, J.-P. Gilson, V. Valtchev, Advances in nanosized zeolites, Nanoscale 5 (2013) 6693–6703, https://doi.org/10.1039/C3NR01629C.
[6] E. Koohsaryan, M. Anbia, Nanosized and hierarchical zeolites: A short review, Chin. J. Catal. 37 (2016) 447–467, https://doi.org/10.1016/S1872-2067(15)61038-5.

[7] L. Tosheva, V.P. Valtchev, Nanozeolites: Synthesis, Crystallization Mechanism, and Applications, Chem. Mater. 17 (2005) 2494–2513, https://doi.org/10.1021/cm047908z.
[8] S. Mintova, J. Grand, V. Valtchev, Nanosized zeolites: Quo Vadis?, Comptes Rendus Chim. 19 (2016) 183–191, https://doi.org/10.1016/j.crci.2015.11.005.
[9] G.-T. Vuong, T.-O. Do, Nanozeolites and Nanoporous Zeolitic Composites: Synthesis and Applications, in: Mesoporous Zeolites, John Wiley & Sons, Ltd, 2015, pp. 79–114. https://doi.org/10.1002/9783527673957.ch3.
[10] J.P. Verduijn, Nanometer-sized molecular sieve crystals or agglomerates and processes for their production, US7767192B1 (2010), https://patents.google.com/patent/US7767192B1/en.
[11] B.J. Schoeman, J. Sterte, J.-E. Otterstedt, Colloidal zeolite suspensions, Zeolites 14 (1994) 110–116, https://doi.org/10.1016/0144-2449(94)90004-3.
[12] H. Hosokawa, K. Oki, Synthesis of Nanosized A-type Zeolites from Sodium Silicates and Sodium Aluminates in the Presence of a Crystallization Inhibitor, Chem. Lett. 32 (2003) 586–587, https://doi.org/10.1246/cl.2003.586.
[13] I. Schmidt, C. Madsen, C.J.H. Jacobsen, Confined Space Synthesis. A Novel Route to Nanosized Zeolites, Inorg. Chem. 39 (2000) 2279–2283, https://doi.org/10.1021/ic991280q.
[14] I. Schmidt, A. Krogh, K. Wienberg, A. Carlsson, M. Brorson, C.J.H. Jacobsen, Catalytic epoxidation of alkenes with hydrogen peroxide over first mesoporous titanium-containing zeolite, Chem. Commun. 21 (2000) 2157–2158, https://doi.org/10.1039/B006460M.
[15] G.-T. Vuong, V.-T. Hoang, D.-T. Nguyen, T.-O. Do, Synthesis of nanozeolites and nanozeolite-based FCC catalysts, and their catalytic activity in gas oil cracking reaction, Appl. Catal. Gen. 382 (2010) 231–239, https://doi.org/10.1016/j.apcata.2010.04.049.
[16] G.-T. Vuong, T.-O. Do, Synthesis of silylated nanozeolites in the presence of organic phase: Two-phase and single-phase methods, Microporous Mesoporous Mater. 120 (2009) 310–316, https://doi.org/10.1016/j.micromeso.2008.11.029.
[17] H. Awala, J.-P. Gilson, R. Retoux, P. Boullay, J.-M. Goupil, V. Valtchev, S. Mintova, Template-free nanosized faujasite-type zeolites, Nat. Mater. 14 (2015) 447–451, https://doi.org/10.1038/nmat4173.
[18] V.P. Valtchev, L. Tosheva, K.N. Bozhilov, Synthesis of Zeolite Nanocrystals at Room Temperature, Langmuir 21 (2005) 10724–10729, https://doi.org/10.1021/la050323e.
[19] E.B. Clatworthy, M. Debost, N. Barrier, S. Gascoin, P. Boullay, A. Vicente, J.-P. Gilson, J.-P. Dath, N. Nesterenko, S. Mintova, Room-Temperature Synthesis of BPH Zeolite Nanosheets Free of Organic Template with Enhanced Stability for Gas Separations, ACS Appl. Nano Mater. 4 (2021) 24–28, https://doi.org/10.1021/acsanm.0c02925.
[20] M. Debost, P.B. Klar, N. Barrier, E.B. Clatworthy, J. Grand, F. Lainé, P. Brazda, L. Palatinus, N. Nesterenko, P. Boullay, S. Mintova, Synthesis of discrete CHA zeolite nanocrystals without organic templates for selective CO_2 capture, Angew. Chem. 59 (2020) 23697–23701, https://doi.org/10.1002/ange.202009397.
[21] J. Shang, G. Li, R. Singh, P. Xiao, J.Z. Liu, P.A. Webley, Determination of Composition Range for "Molecular Trapdoor" Effect in Chabazite Zeolite, J. Phys. Chem. C. 117 (2013) 12841–12847, https://doi.org/10.1021/jp4015146.
[22] H. Sanaeishoar, M. Sabbaghan, F. Mohave, Synthesis and characterization of micro-mesoporous MCM-41 using various ionic liquids as co-templates, Microporous Mesoporous Mater. 217 (2015) 219–224, https://doi.org/10.1016/j.micromeso.2015.06.027.
[23] Y.-K. Ma, S. Rigolet, L. Michelin, J.-L. Paillaud, S. Mintova, F. Khoerunnisa, T.J. Daou, E.-P. Ng, Facile and fast determination of Si/Al ratio of zeolites using FTIR spectroscopy technique, Microporous Mesoporous Mater. 311 (2021) 110683, https://doi.org/10.1016/j.micromeso.2020.110683.
[24] P. Morales-Pacheco, F. Alvarez, L. Bucio, J.M. Domínguez, Synthesis and Structural Properties of Zeolitic Nanocrystals II: FAU-Type Zeolites, J. Phys. Chem. C. 113 (2009) 2247–2255, https://doi.org/10.1021/jp8070713.
[25] M. Handke, M. Kwaśny, Infrared spectroscopic study of octahydridooctasilsesquioxane hydrolytic polycondensation, Vib. Spectrosc. 74 (2014) 127–131, https://doi.org/10.1016/j.vibspec.2014.05.007.
[26] E.M. Flanigen, H. Khatami, H.A. Szymanski, Infrared Structural Studies of Zeolite Frameworks, in: Mol. Sieve Zeolites-I, American Chemical Society, 1974, pp. 201–229. https://doi.org/10.1021/ba-1971-0101.ch016.
[27] X. Guo, D.R. Corbin, A. Navrotsky, Thermodynamics of H_2O and CO_2 Absorption and Guest-Induced Phase Transitions in Zeolite RHO, J. Phys. Chem. C. 122 (2018) 20366–20376, https://doi.org/10.1021/acs.jpcc.8b06070.
[28] G. Engelhardt, D. Michel, High-resolution solid-state NMR of silicates and zeolites, John Wiley & Sons, Chichester, New York, Brisbane, Toronto, Singapore, 1987.